

# Time Domain Resolution of Nanopositioning Systems<sup>\*</sup>

Andrew J. Fleming<sup>\*</sup>

*<sup>\*</sup> School of Electrical Engineering and Computer Science,  
The University of Newcastle, NSW 2300, Australia.  
Email: andrew.fleming@newcastle.edu.au*

---

**Abstract:** In this article, the resolution of a nanopositioning system is defined as the smallest distance between two non-overlapping points. Techniques are then described for estimating the closed-loop resolution from time-domain recordings of the contributing noise sources. Practical guidelines are also discussed to ensure statistically valid estimates. Experimental results show that the resolution of a piezoelectric tube nanopositioner is 2.1 nm with a closed-loop bandwidth of 100 Hz. This figure is identical to previous resolution estimates obtained using more involved frequency-domain measurements.

*Keywords:* Micro-/Nanosystems; Motion Control; Actuator and Sensor Systems; Nanopositioning.

---

## 1. INTRODUCTION

Nanopositioning systems are found in a variety of applications that require positioning with nanometer scale resolution (Devasia et al. (2007)), for example: scanning probe microscopy (Salapaka and Salapaka (2008)), nanofabrication (Mishra et al. (2007); Tseng et al. (2008)), data storage (Sebastian et al. (2008)), cell surgery, beam pointing, and precision optical alignment.

A key performance specification of a nanopositioner, or indeed many other controlled systems, is the resolution. The resolution is essentially the amount of random variation that remains at the output, even when the system is at rest. The resolution is critical for defining the smallest possible dimensions in a manufacturing processes or the smallest measurable features in an imaging application. In the hard drive industry, the standard performance metric for resolution is the track pitch and the standard deviation of the measurement as discussed in Al Mamun and Ge (2005) and Abramovitch and Franklin (2002). However, the main sources of error in a disk drive are due to aeroelastic effects and track eccentricities which are not present in a nanopositioning system.

When defining resolution, it is also important to distinguish between resolution and trueness. While the resolution is a measure of noise and random variation, the trueness defines the position accuracy which includes errors such as sensor non-linearity, abbe error and cosine error. A discussion of nanopositioner accuracy and trueness is contained in Hicks et al. (1997).

In the academic literature, the practices for reporting noise and resolution vary. The most common approach is to predict the closed-loop noise from measurements of the sensor noise, for example Sebastian et al. (2008);

Aphale et al. (2008); Fleming (2010); Fleming et al. (2010). However, this approach can underestimate the true noise since the influence of the high-voltage amplifier is neglected.

In Fleming (2012) the resolution of a nanopositioning system was defined as the minimum distance between two non-overlapping points. This definition is described briefly in Section 2.

Although frequency domain approaches for resolution estimation can be effective, they also require a dynamic signal analyzer and time-consuming averaging processes. In this paper, time-domain techniques are described that allow statistically valid estimates of resolution to be predicted from recordings of the amplifier and sensor noise. This approach is experimentally demonstrated to yield results identical to frequency domain techniques when the closed-loop bandwidth is greater than 10 Hz. For accurate predictions below this frequency, the required recording lengths may become prohibitive long (>100s).

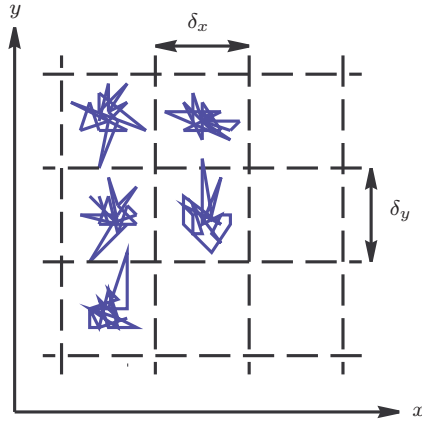
## 2. RESOLUTION AND NOISE

When a nanopositioner has settled to a commanded location, a small amount of random motion remains due to sensor noise, amplifier noise, and external disturbances. The residual random motion means that two adjacent commanded locations may actually overlap, which can cause manufacturing faults or imaging artifacts. To avoid these eventualities, it is critical to know the minimum distance between two adjacent points that can be uniquely identified.

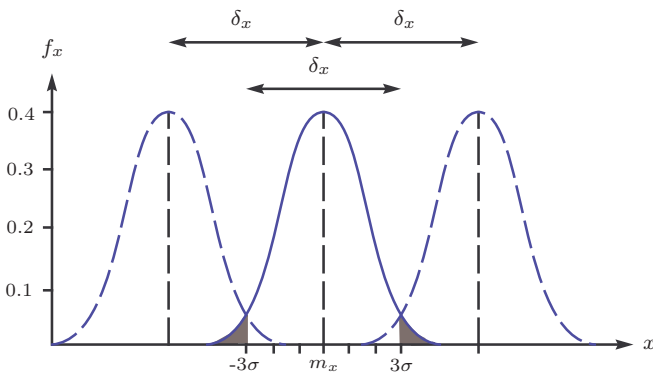
Since the noise sources that contribute to random position errors can have a potentially large dispersion, it is impractically conservative to specify a resolution where adjacent points never overlap. Instead, it is preferable to state the probability that the actual position is within a certain error bound. Consider the example of random positioning

---

<sup>\*</sup> This research was supported by the Australian Research Council Discovery Project (DP0986319)



(a) Two dimensional random motion



(b) The probability density functions of three adjacent points on the x-axis

Fig. 1. The random motion of a two-dimensional nanopositioner. The random motion in the  $x$  and  $y$ -axis is bounded by  $\delta_x$  and  $\delta_y$ . In the  $x$ -axis, the standard deviation and mean are  $\sigma_x$  and  $m_x$  respectively. The shaded areas represent the probability of the position being outside the range specified by  $\delta_x$ .

errors plotted in Figure 1(a). Observe that the peak-to-peak amplitude of random motion is bounded by  $\delta_x$  and  $\delta_y$ , however this range is occasionally exceeded. If the random position variation is assumed to be Gaussian distributed, the probability density functions of three adjacent points, spaced by  $\delta_x$ , are plotted in Figure 1(b). In this example,  $\delta_x$  is equal to  $\pm 3\sigma_x$  or  $6\sigma_x$  which means that 99.7% of the samples fall within the range specified by  $\delta_x$ . Restated, there is a 0.3% chance that the position is exceeding  $\delta_x$  and straying into a neighboring area, this probability is shaded in grey.

For many applications, a 99.7% probability that the position falls within  $\delta_x = 6\sigma_x$  is an appropriate definition for the resolution. To be precise, this definition should be referred to as the  $6\sigma$ -resolution and specifies the minimum spacing between two adjacent points that do not overlap 99.7% of the time. Although there is no international standard for the measurement or reporting of resolution in a positioning system, the ISO 5725 Standard on Accuracy (Trueness and Precision) of Measurement Methods and Results (ISO (1994)) defines precision as the standard deviation (RMS Value) of a measurement. Thus, the  $6\sigma$ -

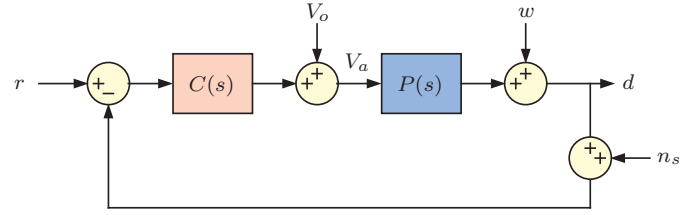


Fig. 2. A single axis feedback control loop with a plant  $P$  and controller  $C$ .

resolution is equivalent to six times the ISO definition for precision.

### 3. NOISE SENSITIVITY FUNCTIONS

The foremost sources of noise in a nanopositioning application are the amplifier noise, sensor noise and external disturbances. To derive the closed-loop position noise, the response of the closed-loop system to each noise source must be considered. In particular, we need to specify the location where each source enters the feedback loop. The amplifier noise  $V_o$  appears at the plant input. In contrast, the external noise  $w$  acts at the plant output, and the sensor noise  $n_s$  disturbs the measurement.

A single axis feedback loop with additive noise sources is illustrated in Figure 2. For the sake of simplicity, the voltage amplifier is considered to be part of the controller. The transfer function from the amplifier voltage noise  $V_o$  to the position  $d$  is the input sensitivity function,

$$\frac{d(s)}{V_o(s)} = \frac{P(s)}{1 + C(s)P(s)}. \quad (1)$$

Likewise, the transfer function from the external noise  $w$  to the position  $d$  is the sensitivity function,

$$\frac{d(s)}{w(s)} = \frac{1}{1 + C(s)P(s)}. \quad (2)$$

Finally, the transfer function from the sensor noise  $n_s$  to the position  $d$  is the negated complementary sensitivity function,

$$\frac{d(s)}{n_s(s)} = \frac{-C(s)P(s)}{1 + C(s)P(s)} \quad (3)$$

### 4. TIME DOMAIN NOISE MEASUREMENTS

With knowledge of the sensitivity functions, the closed-loop position noise can be estimated directly from time-domain measurements. Compared to frequency-domain techniques, the time-domain approach has a number of benefits:

- Simplicity
- A spectrum analyzer is not required
- The distribution histogram can be plotted directly
- No assumptions about the distribution are required to estimate the peak-to-peak value or  $6\sigma$ -resolution

However, there are also a disadvantages:

- It may be difficult to record signals with  $1/f$  noise due to their high dynamic range
- To capture both low- and high-frequency noise, long time records are required with high sampling rate
- There is less insight into the nature of the noise

In summary, time-domain noise recordings are more straight-forward, but lack some of the intuition provided by frequency domain techniques. Time-domain noise measurement techniques are discussed in the following, then applied to a nanopositioning system.

#### 4.1 Total integrated noise

In nanopositioning applications, a useful method for reporting time-domain noise is the total integrated noise, which is the RMS value or standard deviation over a particular measurement bandwidth. If a noise process is assumed to have a constant spectral density of  $\sqrt{A}$  (in nm/ $\sqrt{\text{Hz}}$ ), the total integrated noise can be expressed analytically as,

$$\sigma(f_{bw}) = \sqrt{A} \sqrt{f_{bw}}, \quad (4)$$

where  $\sigma(f_{bw})$  is the RMS value over the measurement bandwidth  $f_{bw}$ . In practice, a white-noise source is filtered by a low-pass system  $G(s)$ . The total integrated noise is now:

$$\sigma(f_{bw}) = \sqrt{\int_0^{f_{bw}} A |G(j2\pi f)|^2 df}. \quad (5)$$

If  $G(s)$  is a first-order filter with cut-off frequency  $f_c$ , the total integrated noise is

$$\sigma(f_{bw}) = \sqrt{A} \sqrt{\int_0^{f_{bw}} \frac{f_c^2}{f^2 + f_c^2} df}. \quad (6)$$

Using the following integral pair from Poularikas (1999) (45.3.6.1),

$$\int \frac{1}{a + bf^2} = \frac{1}{\sqrt{ab}} \tan^{-1} \left( \frac{f\sqrt{ab}}{a} \right), \quad (7)$$

equation (6) reduces to

$$\sigma(f_{bw}) = \sqrt{A} \sqrt{f_c \tan^{-1}(f_{bw} f_c)}. \quad (8)$$

Note that as the measurement bandwidth approaches  $\infty$ ,  $\tan^{-1}(f_{bw} f_c) \rightarrow 1.57$  and  $\sigma(f_{bw})$  approaches the standard expression for the standard deviation of low-pass filtered white noise.

The main benefit of total integrated noise is that it can be measured directly using simple instruments. For example, the plot in Figure 5 can be constructed with a variable cut-off low-pass filter and RMS measuring instrument. The filter order should generally be greater than three to minimize errors resulting from the non-ideal response.

#### 4.2 Estimating the position noise

In the time domain, the process of estimating position noise is similar to frequency domain techniques. Two possible techniques are discussed in the following.

*Direct measurement with an ideal sensor* The most straight-forward and conclusive method for measuring the positioning noise of a nanopositioning system is to measure it directly. However, this approach is not often possible as an additional sensor is required with lower noise and a significantly higher bandwidth than the closed-loop system.

To avoid low-pass filtering and underestimating the noise, the sensor bandwidth must be at least five times greater than the position noise bandwidth. Due to these demanding requirements, direct measurement is rarely an option since a suitable sensor may not be available. If such a sensor is available, a major benefit is that the position noise is not underestimated, which provides a high degree of confidence in the measured noise and also the resolution.

*Prediction based on measured noise* In many cases it is not possible to measure the position noise directly as auxiliary sensors with suitable performance may not be available. In such cases, the position noise can be predicted from measurements of the amplifier and sensor noise. A benefit of this approach is that the the closed-loop noise can be predicted for a number of different bandwidths and controllers, much like frequency domain techniques.

Referring to the feedback diagram in Figure 2, the signals of interest are the amplifier noise  $V_o$  and the sensor noise  $n_s$ . As the position noise is calculated by superposition, the amplifier noise should be measured with the input signal grounded and the output connected to the nanopositioner. Conversely, the sensor noise should be measured with a dedicated test-rig to avoid the influence of external disturbances. If the sensor noise must be measured in-situ, all of the nanopositioner actuators should be disconnected from their sources and short-circuited.

After the constituent noise sources have been recorded, the position noise can be predicted by filtering the noise signals by the sensitivity functions of the control-loop. That is, the position noise is

$$d(t) = n_s(t) \frac{-C(s)P(s)}{1 + C(s)P(s)} + V_o(t) \frac{P(s)}{1 + C(s)P(s)}. \quad (9)$$

The RMS value of the position noise can now be computed and plotted for a range of different controller-gains and closed-loop bandwidths.

Although the data sizes in time domain experiments must be necessarily large to guarantee statistical validity, this is not a serious impediment since a range of numerical tools are readily available for extracting the required information.

For example, in Matlab, the RMS value of a vector  $d$  can be calculated using `RMS=std(d)` or `RMS=sqrt(mean(y.^2))`. The  $6\sigma$ -resolution can be found using the function `Res=2*quantile(abs(d),0.997)`. It is also informative to plot the probability density function using `ksdensity` or with the basic histogram function:

```
xi = linspace(-range,range,Ny);
dx = 2*range/Ny;
[y,x] = hist(d,xi);
plot(x,y/(length(d)*dx))
```

where `-range` and `range` encompass the minimum and maximum values of  $d$  and `Ny` is the number of  $x$ -axis points in the probability density.

#### 4.3 Practical considerations

Many of the considerations for frequency domain noise measurements are also valid for time domain measurements (Fleming (2012)). Of particular importance is the

Record length	100 s
Amplifier bandwidth	$f_V$
Anti-aliasing filter cut-off frequency	$7.5 \times f_V$
Sampling rate	$15 \times f_V$

Table 1. Recommended parameters for time domain noise recordings

need for preamplification and the removal of offset voltages. After a suitable preamplification scheme has been implemented, the position noise can be estimated from recordings of the sensor and amplifier noise. This requires a choice of the recording length and sampling rate. The length of each recording is defined by the lowest spectral component under consideration. With a lower frequency limit of 0.1 Hz, a record length of at least ten times the minimum period is required to obtain a statistically meaningful estimate of the RMS value, which implies a minimum recording length of approximately 100 s. A longer record length is preferable, but may not be practical.

A more rigorous method for selecting the record length is to calculate the estimation variance as a function of the record length. This relationship was described in Fleming and Moheimani (2003), however, assumptions are required about the autocorrelation or power spectral density. In most cases, the simple rule-of-thumb discussed above is sufficient.

When selecting the sampling rate, the highest significant frequency that influences position noise should be considered. Since the sensor noise is low-pass filtered by the closed-loop response of the control loop, the highest significant frequency is usually the bandwidth of the voltage amplifier. An appropriate choice of sampling rate is fifteen times the amplifier bandwidth. This allows a non-ideal anti-aliasing filter to be utilized with a cut-off frequency of five times the amplifier bandwidth. Since the noise power of a first-order amplifier drops to 3.8% at five times the bandwidth, this technique captures the majority of noise power. The recommended parameters for time-domain noise recordings are summarized in Table 1.

## 5. EXPERIMENTAL DEMONSTRATION

### 5.1 Experimental setup

In this section, a time-domain noise analysis is performed on the piezoelectric tube scanner described in Figure 3 and Maess et al. (2008). The frequency response is plotted in Figure 4. The goal is to quantify the achievable resolution as a function of closed-loop bandwidth.

The voltage amplifier used to drive the tube is a Nanonis HVA4 high-voltage amplifier with a gain of 40. To measure the noise, the amplifier input was grounded and the output was amplified by 1000 using an SR560 preamplifier. To remove DC offset, the input of the preamplifier was AC-coupled with a 0.03 Hz cut-off frequency.

The sensor under consideration is an ADE Tech 4810 Gaging Module with 2804 capacitive sensor with a full range of  $\pm 100 \mu\text{m}$  and a sensitivity of  $0.1 \text{ V}/\mu\text{m}$ . To measure the noise, the sensor is mounted inside an Aluminum block

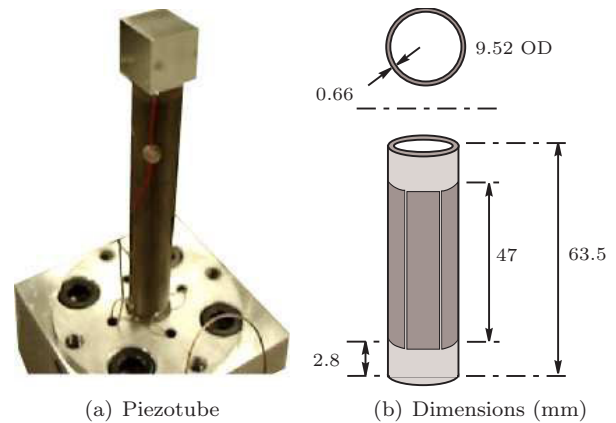


Fig. 3. A piezoelectric tube scanner. The tube tip deflects laterally when an electrode is driven by a voltage source. The sensitivity is  $171 \text{ nm}/\text{V}$  which implies a range of approximately  $68 \mu\text{m}$  with a  $\pm 200 \text{ V}$  excitation.

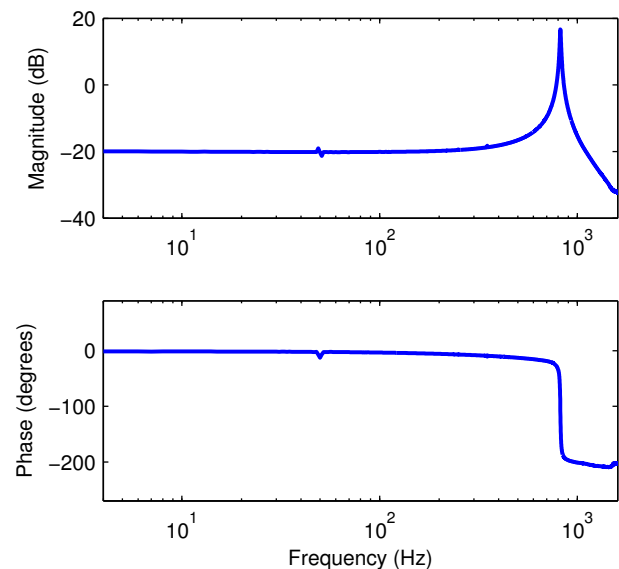


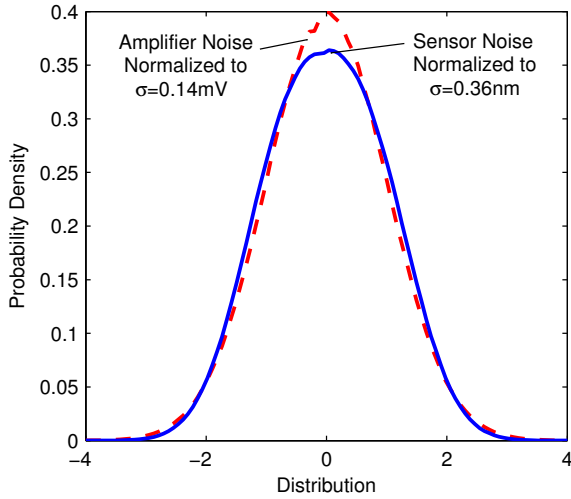
Fig. 4. The lateral frequency response (in  $\mu\text{m}/\text{V}$ ) of the piezoelectric tube scanner pictured in Figure 3. The response was measured from the applied actuator voltage to the resulting displacement.

with a flat-bottomed hole and grub screws to secure the probe and minimize any movement.

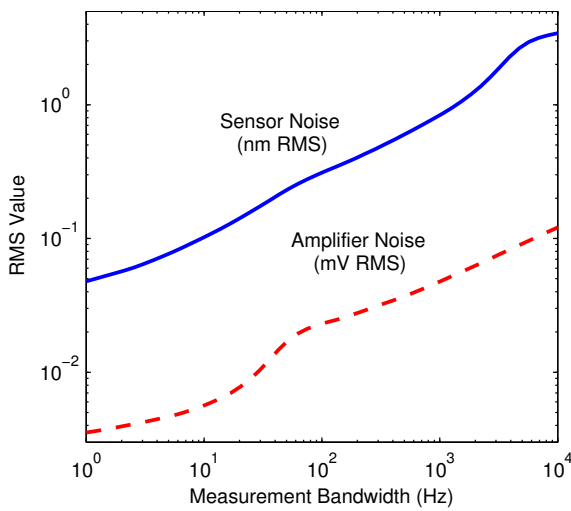
### 5.2 Measurements

Since the bandwidth of the high-voltage amplifier is 2 kHz, the sampling rate is chosen to be 30 kHz. To remove the DC offset, the high-pass cut-off of the preamplifier was set to 0.03 Hz. The preamplifier is also used for anti-aliasing with a cut-off frequency of 10 kHz as recommended in Table 1. With a record length of 100 s, the data contains  $3 \times 10^6$  samples.

The distribution and total integrated noise of the voltage amplifier and sensor are plotted in Figure 5. The RMS value of the amplifier noise is 0.14 mV over the 0.1 Hz to 10 kHz measurement bandwidth which corresponds to



(a) Probability density function



(b) RMS Value vs. measurement bandwidth

Fig. 5. The distribution and total integrated noise of the voltage amplifier and capacitive sensor. Both of the sensors exhibit an approximately Gaussian distribution.

a predicted  $6\sigma$ -resolution of 0.84 mV. The measured  $6\sigma$ -resolution was 0.86 mV which supports the assumption of approximate Gaussian distribution.

The RMS noise and  $6\sigma$ -resolution of the capacitive sensor was measured to be 3.6 nm and 20 nm respectively. The capacitive sensor also exhibits an approximately Gaussian distribution, albeit with a slightly greater dispersion than the voltage amplifier.

### 5.3 Closed-loop position noise

To allow the estimation of closed-loop noise, a system model was identified from the frequency response in Figure 4, the parameters are:

$$P(s) = \frac{0.01151s^2 + 116s + 2.541 \times 10^6}{s^2 + 66.73s + 2.658 \times 10^7} \mu\text{m/V}. \quad (10)$$

For the sake of demonstration, a controller is chosen that represents the characteristics of a wide variety of model-

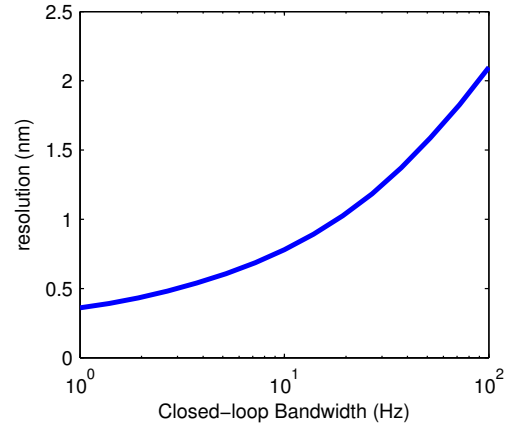


Fig. 6. The  $6\sigma$ -resolution versus closed-loop bandwidth derived from time-domain measurements. This plot closely matches the frequency-domain result in Fleming (2012) except when the closed-loop bandwidth is less than 10 Hz. For greater accuracy when the closed-loop bandwidth is less than 10 Hz, a longer data recording is required.

based and ad-hoc control schemes. The transfer function is an integrator combined with an inverse model of the plant,

$$C(s) = \frac{\alpha}{s} \frac{1}{P(s)}. \quad (11)$$

The resulting loop-gain  $C(s)P(s)$  is approximately an integrator, so stability is guaranteed and the closed-loop bandwidth is  $\alpha$  rad/s. With such a controller it is now possible to examine the noise performance of feedback systems over a wide bandwidth.

The position noise can now be simulated using the noise recordings and equation (9). At low closed-loop bandwidth, the transient response time of the system is significant. For this reason, only the second half of the simulated output is used to calculate the resolution. For the same reason, it is not practical to simulate a closed-loop bandwidth less than 1 Hz. This is an additional disadvantage of time-domain approaches.

The predicted resolution is plotted against closed-loop bandwidth in Figure 6. This plot closely resembles a similar plot acquired from frequency domain data in Fleming (2012). The time-domain results are compared to the frequency domain results in Table 2. With a closed-loop bandwidth of 100 Hz, the predictions are identical, however, at low closed-loop bandwidth, some discrepancy exists. This is due to the long transient response which tends to underestimate the positioning noise at very low closed-loop bandwidths. If necessary, a more accurate result can be achieved by significantly increasing the recording length, however this is not usually desirable or practical.

Bandwidth	Frequency Domain	Time Domain
100 Hz	2.2 nm	2.1 nm
10 Hz	0.92 nm	0.78 nm
1 Hz	0.55 nm	0.36 nm

Table 2. The predicted closed-loop resolution using frequency and time-domain measurements.

## 6. CONCLUSIONS

In nanopositioning applications, an appropriate definition for resolution is the bound that encloses 99.7% of position observations. This is equivalent to the minimum distance between two non-overlapping points. If the contributing noise sources are Gaussian random processes, the peak-to-peak variation is equal to six times the standard deviation, which is referred to as the  $6\sigma$ -resolution.

In this article, the closed-loop position noise was predicted from time-domain measurements of the amplifier and sensor noise. This approach eliminates the need for a spectrum analyzer and time consuming averaging processes.

To obtain valid time-domain resolution estimates, the key data requirements are a sampling frequency at least fifteen times the amplifier bandwidth and a recording length of at least 100s. These parameters were experimentally demonstrated to provide similar predictions to frequency domain techniques when the closed-loop bandwidth is greater than 10 Hz. If accurate predictions below 10 Hz are required, frequency domain approaches may be more suitable.

## REFERENCES

- (1994). ISO 5725 - accuracy (trueness and precision) of measurement methods and results, interational organization for standardization.
- Abramovitch, D. and Franklin, G. (2002). A brief history of disk drive control. *IEEE Control Systems*, 22(3), 28–42. doi:10.1109/MCS.2002.1003997.
- Al Mamun, A. and Ge, S.S. (2005). Precision control of hard disk drives. *IEEE Control Systems*, 25(4), 14–19. doi:10.1109/MCS.2005.1499384.
- Aphale, S.S., Bhikkaji, B., and Moheimani, S.O.R. (2008). Minimizing scanning errors in piezoelectric stack-actuated nanopositioning platforms. *IEEE Transactions on Nanotechnology*, 7(1), 79–90.
- Devasia, S., Eleftheriou, E., and Moheimani, S.O.R. (2007). A survey of control issues in nanopositioning. *IEEE Transactions on Control Systems Technology*, 15(5), 802–823.
- Fleming, A.J. (2010). Nanopositioning system with force feedback for high-performance tracking and vibration control. *IEEE Transactions on Mechatronics*, 15(3), 433–447.
- Fleming, A.J. (2012). Estimating the resolution of nanopositioning systems from frequency domain data. In *Proc. IEEE International Conference on Robotics and Automation*, 4786–4791. St. Paul, MN.
- Fleming, A.J., Aphale, S.S., and Moheimani, S.O.R. (2010). A new method for robust damping and tracking control of scanning probe microscope positioning stages. *IEEE Transactions on Nanotechnology*, 9(4), 438–448. doi:10.1109/TNANO.2009.2032418.
- Fleming, A.J. and Moheimani, S.O.R. (2003). Adaptive piezoelectric shunt damping. *IOP Smart Materials and Structures*, 12(1), 18–28.
- Hicks, T.R., Atherton, P.D., Xu, Y., and McConnell, M. (1997). *The nanopositioning book*. Queensgate Instruments Ltd., Berkshire, UK.
- Maess, J., Fleming, A.J., and Allgöwer, F. (2008). Simulation of dynamics-coupling in piezoelectric tube scanners by reduced order finite element models. *Review of Scientific Instruments*, 79, 015105(1–9). doi:10.1063/1.2826428.
- Mishra, S., Coaplen, J., and Tomizuka, M. (2007). Precision positioning of wafer scanners. segmented iterative learning control for nonrepetitive disturbances. *IEEE Control Systems*, 27(4), 20–25. doi:10.1109/MCS.2007.384130.
- Poularikas, A.D. (1999). *The handbook of formulas and tables for signal processing*. CRC Press, Boca Raton, FL.
- Salapaka, S.M. and Salapaka, M.V. (2008). Scanning probe microscopy. *IEEE Control Systems*, 28(2), 65–83.
- Sebastian, A., Pantazi, A., Pozidis, H., and Elefthriou, E. (2008). Nanopositioning for probe-based data storage. *IEEE Control Systems*, 28(4), 26–35.
- Tseng, A.A., Jou, S., Notargiacomo, A., and Chen, T.P. (2008). Recent developments in tip-based nanofabrication and its roadmap. *Journal of Nanoscience and Nanotechnology*, 8(5), 2167–2186.